







**BRIEF CONCLUSIVE REPORT**

# Quantitative single-molecule imaging of TNFR1 reveals zafirlukast as antagonist of TNFR1 clustering and TNF $\alpha$ -induced NF- $\kappa$ B signaling

Nadine Weinelt<sup>1</sup>  | Christos Karathanasis<sup>2</sup>  | Sonja Smith<sup>1</sup>  |  
 Juliane Medler<sup>3</sup>  | Sebastian Malkusch<sup>4</sup>  | Simone Fulda<sup>1,5,6</sup>  |  
 Harald Wajant<sup>3</sup>  | Mike Heilemann<sup>2</sup>  | Sjoerd J. L. van Wijk<sup>1</sup> 

<sup>1</sup>Institute for Experimental Cancer Research in Pediatrics, Goethe University, Frankfurt am Main, Germany

<sup>2</sup>Institute of Physical and Theoretical Chemistry, Goethe University, Frankfurt am Main, Germany

<sup>3</sup>Division of Molecular Internal Medicine, Department of Internal Medicine II, University Hospital Würzburg, Auverhaus, Würzburg, Germany

<sup>4</sup>Institute of Clinical Pharmacology, Goethe-University, Frankfurt am Main, Germany

<sup>5</sup>German Cancer Consortium (DKTK), Partner site Frankfurt am Main, Germany

<sup>6</sup>German Cancer Research Centre (DKFZ), Heidelberg, Germany

**Correspondence**

Sjoerd J. L. van Wijk, Institute for Experimental Cancer Research in Pediatrics, Goethe-University Frankfurt, Komturstasse, 3a, Frankfurt am Main 60528, Germany.  
 Email: s.wijk@kinderkrebsstiftung-frankfurt.de

**Abstract**

TNFR1 is a crucial regulator of NF- $\kappa$ B-mediated proinflammatory cell survival responses and programmed cell death (PCD). Deregulation of TNF $\alpha$ - and TNFR1-controlled NF- $\kappa$ B signaling underlies major diseases, like cancer, inflammation, and autoimmune diseases. Therefore, although being routinely used, antagonists of TNF $\alpha$  might also affect TNFR2-mediated processes, so that alternative approaches to directly antagonize TNFR1 are beneficial. Here, we apply quantitative single-molecule localization microscopy (SMLM) of TNFR1 in physiologic cellular settings to validate and characterize TNFR1 inhibitory substances, exemplified by the recently described TNFR1 antagonist zafirlukast. Treatment of TNFR1-mEos2 reconstituted TNFR1/2 knockout mouse embryonic fibroblasts (MEFs) with zafirlukast inhibited both ligand-independent preligand assembly domain (PLAD)-mediated TNFR1 dimerization as well as TNF $\alpha$ -induced TNFR1 oligomerization. In addition, zafirlukast-mediated inhibition of TNFR1 clustering was accompanied by deregulation of acute and prolonged NF- $\kappa$ B signaling in reconstituted TNFR1-mEos2 MEFs and human cervical carcinoma cells. These findings reveal the necessity of PLAD-mediated, ligand-independent TNFR1 dimerization for NF- $\kappa$ B activation, highlight the PLAD as central regulator of TNF $\alpha$ -induced TNFR1 oligomerization, and demonstrate that TNFR1-mEos2 MEFs can be used to investigate TNFR1-antagonizing compounds employing single-molecule quantification and functional NF- $\kappa$ B assays at physiologic conditions.

**KEYWORDS**

Single-Molecule Localization Microscopy (SMLM), Pre-Ligand Assembly Domain (PLAD), Cysteine-Rich Domain (CRD), CysLTR1

**1 | INTRODUCTION**

Careful control of the balance between survival and cell death is essential for normal organismal development and tissue homeostasis and is often disturbed in pathophysiologic conditions, like tumor formation,

autoimmunity and infection diseases.<sup>1-3</sup> Cell fate responses are critically regulated by death receptors (DRs), such as TNFR1, a prototypical 55-kDa DR of the TNFR superfamily (TNFRSF), that contain an intracellular death domain (DD).<sup>3-6</sup> TNFR1 comprises 4 cysteine-rich domains (CRDs) in the extracellular domain, a transmembrane region

Abbreviations: cIAP, cellular Inhibitor of Apoptosis; CRD, cysteine-rich domains; Cxcl1, C-X-C motif chemokine 1; CysLTR1, cysteinyl leukotriene receptor 1; DD, death domain; DR, death receptor; FRET, Förster resonance energy transfer; KO, knockout; LT $\alpha$ , lymphotoxin- $\alpha$ ; MEF, mouse embryonic fibroblast; MLKL, mixed lineage kinase domain-like protein; PCD, programmed cell death; PLAD, preligand assembly domain; RIPK1, receptor-interacting serine/threonine-protein kinase-1; RIPK3, receptor-interacting serine/threonine protein kinase 3; SC, signaling complex; SMLM, single-molecule localization microscopy; TIRF, total internal reflection fluorescence; TNFR1, TNF receptor 1; TNFRSF, TNFR superfamily; TRADD, TNFR1-associated death domain protein; TRAF, TNFR-associated factor.

This is an open access article under the terms of the Creative Commons Attribution-NonCommercial-NoDerivs License, which permits use and distribution in any medium, provided the original work is properly cited, the use is non-commercial and no modifications or adaptations are made.

© 2020 The Authors. *Journal of Leukocyte Biology* published by Wiley Periodicals, Inc. on behalf of Society for Leukocyte Biology

and an intracellular domain with the C-terminally located DD.<sup>3-6</sup> TNFR1 is partially predimerized through the preligand assembly domain (PLAD) in its distal CRD1 in the absence of ligands.<sup>7</sup> Binding of TNF $\alpha$  or lymphotoxin- $\alpha$  (LT $\alpha$ ) to TNFR1 occurs through ligand-receptor interactions in CRD2-CRD3, leading to clustering of ligand-bound TNFR1.<sup>6-10</sup> By doing so, TNF $\alpha$  binding induces rearrangements in the TNFR1 DD, leading to the formation of TNFR1-associated signaling complexes (SC), containing TNFR1-associated death domain protein (TRADD), receptor-interacting serine/threonine-protein kinase-1 (RIPK1), TNFR-associated factor 2 (TRAF2), cellular Inhibitor of apoptosis proteins (cIAP1/2), and various RIPK1 and TRAF2-associated proteins.<sup>1-4</sup> TNF $\alpha$  binding to TNFR1 generally induces prosurvival NF- $\kappa$ B, JNK, p38-MAPK, and ERK signaling.<sup>2,4</sup> However, depending on the stimulus and cellular context, TNFR1 activation can also induce programmed cell death (PCD), like caspase-dependent apoptotic cell death. This is clearly illustrated, for example, by Second mitochondria-derived activator of caspase mimetic-induced degradation of cIAP1/2, leading to NF- $\kappa$ B-inducing kinase stabilization and creating autocrine TNF $\alpha$ -TNFR1 signaling loops that induce loss of cell viability in many types of tumor cells, like breast cancer.<sup>1,2,8,11-13</sup>

TNF $\alpha$  is a central inflammatory cytokine produced by many different cell types, including macrophages, lymphocytes, and neutrophils<sup>4,14</sup> and is required to control inflammatory processes and bacterial and viral infection, but also promotes autoimmune diseases and cancer.<sup>14,15</sup> Indeed, because of their central role in autoimmunity, TNF $\alpha$  inhibitors are powerful therapeutics in the treatment of rheumatoid arthritis, psoriasis, and inflammatory bowel disease.<sup>16</sup> Unfortunately, occasional side effects are reported upon inhibition of TNF $\alpha$ , including life-threatening infections, for example, reactivation of hepatitis B and tuberculosis.<sup>17,18</sup> Moreover, TNF $\alpha$  blockers fail to show efficacy in diseases where TNF $\alpha$  has been strongly implicated as promotor of disease, such as multiple sclerosis and heart failure.<sup>19,20</sup> This may reflect the fact that TNF $\alpha$  blockers prevent not only TNFR1 signaling but also activation of TNFR2, which can elicit potent anti-inflammatory activity via stimulation of regulatory T-cells, regulatory B-cells, and myeloid-derived suppressor cells.<sup>21,22</sup> Therefore, there is interest in developing alternative therapeutic interventions that target TNFR1 itself instead of TNF $\alpha$ . Indeed, recent studies have described small-molecule inhibitors of TNFR1 that target TNFR1 preligand dimerization or conformational rearrangements of preassembled TNFR1 dimers.<sup>13,23</sup> Despite this, experimental approaches and methodologies necessary to understand, validate and potentially optimize these small-molecule TNFR1 antagonists remain sparse and are currently limited to Förster resonance energy transfer (FRET) dimerization analysis of GFP- and RFP-tagged TNFR1 lacking the intracellular DD.<sup>13,23</sup> Using this FRET-based system, the cysteinyl leukotriene receptor 1 (CysLTR1) antagonist zafirlukast has been identified as a competitive inhibitor of TNFR1 PLAD dimerization.<sup>23</sup> Zafirlukast and other CysLTR1 antagonists are clinically applied to treat asthma and are used as anti-inflammatory drugs in cystic fibrosis.<sup>24,25</sup> Furthermore, zafirlukast has been reported to inhibit TNF $\alpha$ -induced endothelial cell inflammation<sup>26</sup> and to inhibit proliferation of tumor cells.<sup>25</sup>

Recent developments in microscopy and image analysis now allow studying protein complexes directly in cells and with a near-molecular spatial resolution.<sup>15,27</sup> Single-molecule localization microscopy (SMLM) in combination with the analysis of fluorophore photocycles<sup>28</sup> and theoretically derived models<sup>29,30</sup> allows for quantitative imaging of receptor complexes in cells.<sup>31</sup> For example, quantitative SMLM revealed the distributions of the oligomeric states of various membrane receptors<sup>10,32</sup> and showed a dynamic equilibrium of oligomeric states for Toll-like receptor 4.<sup>33</sup>

Here, we investigate the applicability of our previously developed quantitative TNFR1 single-molecule super-resolution imaging platform<sup>34</sup> to validate the mode of action of zafirlukast on full-length human TNFR1 in intact cells. Using this platform, we demonstrate and confirm that zafirlukast inhibits ligand-independent TNFR1 PLAD-PLAD-mediated dimerization as well as TNF $\alpha$ -induced higher-order TNFR1 clustering. Additionally, prevention of TNFR1 clustering was further accompanied by inhibition of acute TNF $\alpha$ -induced inhibitor of  $\kappa$ B  $\alpha$  (I $\kappa$ B $\alpha$ ) phosphorylation and NF- $\kappa$ B-mediated gene expression and cytokine secretion in TNFR1-mEos2 MEFs and HeLa cells.

## 2 | MATERIALS AND METHODS

### 2.1 | Cell lines, antibodies, and reagents

SV40 large T-antigen immortalized TNFR1/2 wild-type (WT) and knockout (KO) mouse embryonic fibroblasts (MEFs) stably reconstituted with full-length human TNFR1-mEos2 (TNFR1/2 KO + TNFR1-mEos2) have been described in detail previously<sup>34</sup> and maintained in RPMI (Life Technologies, Inc., Eggenstein, Germany), supplemented with 10% FBS (Biochrom, Berlin, Germany), 1% Glutamax (Life Technologies), and 1% penicillin/streptomycin (Invitrogen, Thermo Fisher Scientific, Karlsruhe, Germany). The human cervical carcinoma HeLa cell line was obtained from DSMZ (Braunschweig, Germany) and cultured in DMEM (Life Technologies), supplemented with 10% FBS (Biochrom), 1% Glutamax (Life Technologies), 1% sodium pyruvate (Gibco, Thermo Fisher Scientific), and 1% penicillin/streptomycin (Invitrogen). All cell lines were maintained at 37°C with 5% CO<sub>2</sub> and regularly tested for mycoplasma infections.

Zafirlukast and bardoxolone methyl were purchased from SelleckChem (Munich, Germany), recombinant human TNF $\alpha$  was obtained from Peprotech (Hamburg, Germany), and Biochrom and all other chemicals were obtained from Sigma-Aldrich (Deisenhofen, Germany) or Carl Roth (Karlsruhe, Germany), unless stated otherwise.

Antibodies used in this study were monoclonal anti-vinculin (V9131; Sigma-Aldrich), anti-I $\kappa$ B $\alpha$  (#9242; Cell Signaling Technology, Frankfurt am Main, Germany), and anti-phospho-I $\kappa$ B $\alpha$  (Ser32, 14D4, 2859; Cell Signaling Technology).

### 2.2 | Cell lysis and Western blotting

Cells were washed 2 times with ice-cold PBS and lysed in lysis buffer (30 mM Tris-HCl pH 7.4, 150 mM NaCl, 1% (v/v) Triton X-100 and 10% (v/v) glycerol), supplemented with Complete Protease Inhibitors

(Roche, Mannheim, Germany). Lysates were incubated on ice for 20 min and centrifuged at  $16,000 \times g$  at  $4^{\circ}\text{C}$  for 20 min. Cleared cell lysates were boiled in  $2\times$  Laemmli sample buffer (4% (w/v) SDS, 20% (v/v) glycerol, 120 mM Tris-HCl pH 6.8, 0.02% bromophenol blue), and resolved on SDS-PAGE followed by immunoblotting and detection with goat anti-mouse IgG or goat anti-rabbit IgG (Abcam, Cambridge, UK) conjugated to HRP and ECL (Thermo Fisher Scientific).

## 2.3 | Cytokine stimulations

To analyze the effects of zafirlukast on  $\text{TNF}\alpha$ -induced NF- $\kappa\text{B}$  signaling in TNFR1/2 WT, TNFR1/2 KO, TNFR1/2 KO + TNFR1-mEos2 MEFs and HeLa,  $7.5 \times 10^5$  cells were seeded in sterile 6-well plates. Cells were serum-starved for 3 h in medium without FBS at  $37^{\circ}\text{C}$ , followed by incubation with DMSO or zafirlukast (100  $\mu\text{M}$ ) for 1 h at  $37^{\circ}\text{C}$ . After that, cells were stimulated with  $\text{TNF}\alpha$  (20 ng/ml) for the indicated time points at  $37^{\circ}\text{C}$ , followed by medium removal and further processing of the cells.

## 2.4 | Quantitative real-time PCR

Total RNA was isolated using the PeqGOLDTotal RNA Kit (Peqlab, Erlangen, Germany), according to the supplier's instructions. Using 1  $\mu\text{g}$  of total RNA, cDNA was synthesized with help of the RevertAid H Minus First Strand cDNA Synthesis Kit (MBI Fermentas, St. Leon-Roth, Germany), according to the manufacturer's instructions. NF- $\kappa\text{B}$  target gene expression levels were quantified using SYBR Green-based quantitative real-time PCR (Applied Biosystems, Darmstadt, Germany) using a 7900 GR Fast Real-time PCR system (Applied Biosystems). Data were normalized against 28S-rRNA, RPLP0, or GAPDH expression and relative gene expression levels were calculated compared with housekeeping genes using the  $\Delta\Delta\text{Ct}$ -method. All primers were purchased from Eurofins (Hamburg, Germany) and primer sequences are available upon request from the corresponding author.

## 2.5 | Cytokine measurements

The effect of zafirlukast on cytokine induction upon  $\text{TNF}\alpha$  stimulation in TNFR1/2 WT, TNFR1/2 KO, and TNFR1/2 KO + TNFR1-mEos2 MEFs or HeLa cells was analyzed using Cxcl1 or IL-8 ELISA, respectively. For this,  $2.0 \times 10^4$  cells/well were seeded in 96-well plates in serum-free medium and on the next day, cells were preincubated for 30 min with the indicated amounts of zafirlukast, followed by stimulation with the indicated concentrations of  $\text{TNF}\alpha$ , in triplicates. C-X-C motif chemokine 1 (Cxcl1) levels in the supernatants of TNFR1/2 WT, TNFR1/2 KO, and TNFR1/2 KO + TNFR1-mEos2 MEFs were determined after 2 and 4 h using the Mouse Cxcl1/KC DuoSet<sup>®</sup> ELISA kit (R&D Systems, Abingdon, UK) according to the manufacturer's instructions. Absorbance at 450 nm was measured using an Infinite M200 microplate reader (Tecan, Crailsheim, Germany). The data were normalized to the percentage of viable cells as determined by propidium iodide/Hoechst 33342 staining, as described previously.<sup>34</sup> The amount of IL-8 in the supernatants of HeLa cells was detected after 8 h incuba-

tion by using BD OptEIA<sup>™</sup> IL-8 ELISA kit (BD Biosciences, Heidelberg, Germany) according to the manufacturer's instructions. Absorbance at 405 nm was measured with a LUMO-photometer (Anthos Labtec Instruments, Wals, Austria).

## 2.6 | Sample preparation for super-resolution microscopy

Prior to cell seeding, glass slides were cleaned for 15 min in isopropanol (VWR, Darmstadt, Germany) in an ultrasonic bath, then washed with water, dried with  $\text{N}_2$ , and cleaned in a plasma cleaner with  $\text{N}_2$  (Diener Electronic, Ebhausen, Germany) for 15 min. Plasma-cleaned slides were coated with 0.8 mg/ml poly (L-lysine)-poly(ethylene glycol) (Merck, Darmstadt, Germany)-PEG (Rapp Polymere, Tübingen, Germany)-RGD for 90 min at room temperature. Slides were washed with water, dried under  $\text{N}_2$  and 8-well flexiperm chambers (Greiner, Oberursel, Germany) were mounted on the clean and coated glass slides. TNFR1/2 KO + TNFR1-mEos2 MEFs were seeded in serum-starvation medium (RPMI 1640, 1% GlutaMAX, 100  $\mu\text{g}/\text{ml}$  streptomycin, 100  $\mu\text{g}/\text{ml}$  gentamicin, 100 U/ml penicillin), pretreated with 100  $\mu\text{M}$  zafirlukast or with 1% DMSO for 30 min at  $37^{\circ}\text{C}$ . Cells were cooled to  $4^{\circ}\text{C}$ , and incubated with AlexaFluor647-labelled SNAP-tagged  $\text{TNF}\alpha$  (100 ng/ml) for 30 min at  $4^{\circ}\text{C}$ . Treated cells were fixed in 4% methanol-free formaldehyde (ThermoFisher), 0.2% glutaraldehyde (Merck) and 400 mM sucrose in sterile filtered PBS for 15 min at room temperature.

## 2.7 | Single-molecule localization microscopy

SMLM experiments were performed on a home-built microscope<sup>28</sup> in Total Internal Reflection Fluorescence (TIRF) mode. mEos2 was photo-converted with 405 nm light (LBX-405-50-CSB-PP; Oxxius, Lannion, France; intensity of 0–8  $\text{mW}/\text{cm}^2$ ) and excited at 568 nm (Sapphire 568 LP; Coherent, Dieburg, Germany; intensity of 0.21  $\text{kW}/\text{cm}^2$ ). Alexa-Fluor647 was excited at 638 nm (LBX-638-180; Oxxius; intensity of 4.6  $\text{W}/\text{cm}^2$ ). The excitation light was combined using dichroic mirrors (AHF, Germany) and focused onto the back focal plane of a  $100\times$  oil immersion objective (PLAPO 100  $\times$  TIRFM,  $\text{NA} \geq 1.45$ , Olympus, Düsseldorf, Germany) mounted on an inverted microscope (IX71; Olympus). The emission light passed appropriate filters (BrightLine HC 590/20 or ET 700/75 (AHF, Tübingen, Germany)) and was directed on an electron-multiplying charge-coupled device (EMCCD; Andor Ixon, Ireland). Image stacks of 40,000 to 80,000 frames were recorded using an exposure time of 100 ms, an electron multiplying gain of 200 and a preamplifier gain of 1.

## 2.8 | Data analysis

SMLM image stacks were analyzed with rapidSTORM<sup>35</sup> and LAMA<sup>36</sup> as described previously.<sup>34</sup> The number of TNFR1-mEos2 emission events in each cluster was determined with a threshold of 63 photons, and mEos signals within a radius of 90 nm in following camera frames were grouped as single localization by a Kalman-filtering algorithm

implemented in rapidSTORM. For each experimental condition, at least 10 cells from at least 3 independent experiments were analyzed. The parameters for fitting were determined experimentally and validated by analyzing known monomeric (CD86-mEos2) and dimeric (CTLA4-mEos2) membrane proteins,<sup>28</sup> expressed in the same MEF background and under equal experimental conditions used in the present study. Photoactivated localization microscopy data were fit with monomer and dimer models leading to 2 different possibilities to analyze the data (monomer or dimer). Parameter estimation was realized by optimizing the likelihood of a family of mixture models comprising all possible combinations of molecular oligomeric states. The model selection was performed for optimal quality of fit and the appropriateness of the number of free parameters occurred based on using the Bayesian information criterion, as described before.<sup>34</sup>

## 2.9 | Statistical analysis

Statistical significance was calculated using Student's *t*-test (2-tailed distribution, 2-sample and equal variance). Data are presented as mean  $\pm$  SD of 3 or more independent experiments, performed in duplicate, unless stated otherwise. *P* values < 0.05 were considered significant and indicated as follows: \**P* < 0.05; \*\**P* < 0.01; \*\*\**P* < 0.001.

## 3 | RESULTS AND DISCUSSION

Antagonists that interfere with TNF $\alpha$ -induced NF- $\kappa$ B signaling by direct inhibition of TNFR1 clustering are promising drug candidates. However, with the current experimental methodologies it remains challenging to directly identify, validate, and test such TNFR1 inhibitory substances. One recently described exception is a FRET-based system in which GFP- and RFP-tagged TNFR1 that lack the intracellular DD are stably expressed in HEK293T cells and applied to screen for chemical substances that reduce PLAD-mediated FRET dimerization.<sup>13,23</sup> However, the presence of endogenous TNFR1 and the truncation of the intracellular DD limits the functional analysis of TNFR1 activation in NF- $\kappa$ B in these settings. Previously, we developed a stable genetic system that enables quantitative SMLM<sup>27</sup> imaging of full-length human TNFR1 molecules at the intact cellular membrane in physiologic settings with single molecule resolution.<sup>34</sup> This system, in which TNFR1/2 KO MEFs are stably reconstituted with full-length human TNFR1-mEos2, allows for quantitative single-molecule imaging of the TNFR1 clustering patterns in the cell membrane. Statistical analysis of TNFR1 distributions revealed PLAD-mediated ligand-independent TNFR1 dimerization and higher order clustering of TNFR1 upon ligand exposure. Furthermore, we have comprehensively confirmed the functionality of the full-length reconstituted human TNFR1 in these cells, including the absence of TNFR1 auto-activation, reestablishment of NF- $\kappa$ B signaling as well as restoration of TNF $\alpha$ -induced PCD responses.<sup>34</sup> Therefore, we reasoned that this genetic stable TNFR1 imaging platform might be a useful reference system to confirm and evaluate the molecular mechanisms of TNFR1-antagonizing molecules. Previously, we have demonstrated that

serum-starved and ligand-free TNFR1-mEos2 adopt a monomeric: dimeric membrane distribution of 66%  $\pm$  4%: 34%  $\pm$  4%, mediated by PLAD-PLAD interactions.<sup>34</sup> Incubating these cells with TNF $\alpha$  induced prominent 3-state TNFR1 membrane clustering patterns, consisting of 13%  $\pm$  2% monomers, 64%  $\pm$  2% trimers, and 23%  $\pm$  3% nonamers (Fig. 1A).<sup>34</sup> To evaluate the usefulness of these molecular TNFR1-mEos2 patterns as read-out to test TNFR1 antagonists, TNFR1/2 KO + TNFR1-mEos2 MEFs were serum-starved and cooled to 4°C to prevent TNFR1 internalization followed by treatment with zafirlukast. Strikingly, this induced a complete reduction of ligand-independent, PLAD-mediated TNFR1-mEos2 dimerization, yielding a monomer: dimer distribution of 90%  $\pm$  3%: 10%  $\pm$  3% (Fig. 1B). Surprisingly, pretreating TNFR1/2 KO + TNFR1-mEos2 MEFs with zafirlukast, followed by TNF $\alpha$  stimulation also completely abrogated ligand-induced higher-order TNFR1 clustering, leading to a monomer: dimer patterning of 91%  $\pm$  3%: 9%  $\pm$  3% TNFR1 molecules (Fig. 1C). Together, these findings confirmed and validated zafirlukast as an inhibitor of PLAD-mediated ligand-independent TNFR1 clustering as well as TNF $\alpha$ -induced higher order TNFR1 clustering in the mammalian cell membrane. Indeed, the mutation K32A, located in CRD1 of TNFR1 and expected to disturb zafirlukast binding based on molecular modeling<sup>23</sup> yielded monomeric TNFR1 that failed to undergo PLAD-mediated dimerization and ligand-induced oligomerization.<sup>34</sup> These observations not only further confirmed the fundamental relevance of PLAD-PLAD-mediated interactions for TNFR1 presignaling dimerization, but also highlight the PLAD as an essential component for the assembly of TNF $\alpha$ -induced higher order TNFR1 clusters.

In addition, these quantitative SMLM experiments confirm the applicability of the previously developed TNFR1-mEos2 imaging platform<sup>34</sup> in validating and characterizing the molecular mechanisms of TNFR1 clustering antagonists. Given the recent developments in applying single-molecule imaging in (semi) high-throughput/high-content settings,<sup>37</sup> SMLM-based quantitative TNFR1 imaging could be adapted for screening purposes as well in the future.

Ligand-induced clustering of TNFR1 is considered as a key event of TNFR1 activation inducing proinflammatory NF- $\kappa$ B signaling responses in many cell types.<sup>1,2,4</sup> Therefore, we asked whether zafirlukast-mediated inhibition of TNF $\alpha$ -induced TNFR1 clustering also affects TNFR1 downstream signaling in the same TNFR1-mEos2 reconstituted MEFs that were used for TNFR1 imaging. Treating TNFR1/2 KO + TNFR1-mEos2 MEFs with TNF $\alpha$  in the absence of zafirlukast induced functional NF- $\kappa$ B responses characterized by phosphorylation of I $\kappa$ B $\alpha$ , followed by I $\kappa$ B $\alpha$  degradation (Fig. 2A, top, lanes 1–6). As anticipated, these signaling patterns were similar to those observed for TNF $\alpha$ -treated TNFR1/2 WT MEFs, although to a lesser extent as those observed for TNFR1/2 KO + TNFR1-mEos2 (Fig. 2A, bottom, lanes 1–6) and were completely absent in TNFR1/2 KO MEFs (Supplemental Fig. 1, lanes 1–3). Interestingly, pretreatment of TNFR1/2 KO + TNFR1-mEos2 MEFs with zafirlukast delayed the appearance of phosphorylated I $\kappa$ B $\alpha$  and inhibited I $\kappa$ B $\alpha$  degradation after 15 min of ligand stimulation (Fig. 2A, top, lanes 7–12). Intriguingly, these effects were also observed in zafirlukast-treated TNFR1/2 WT MEFs (Fig. 2A, bottom, lanes 7–12) and, as expected, were absent in TNFR1/2

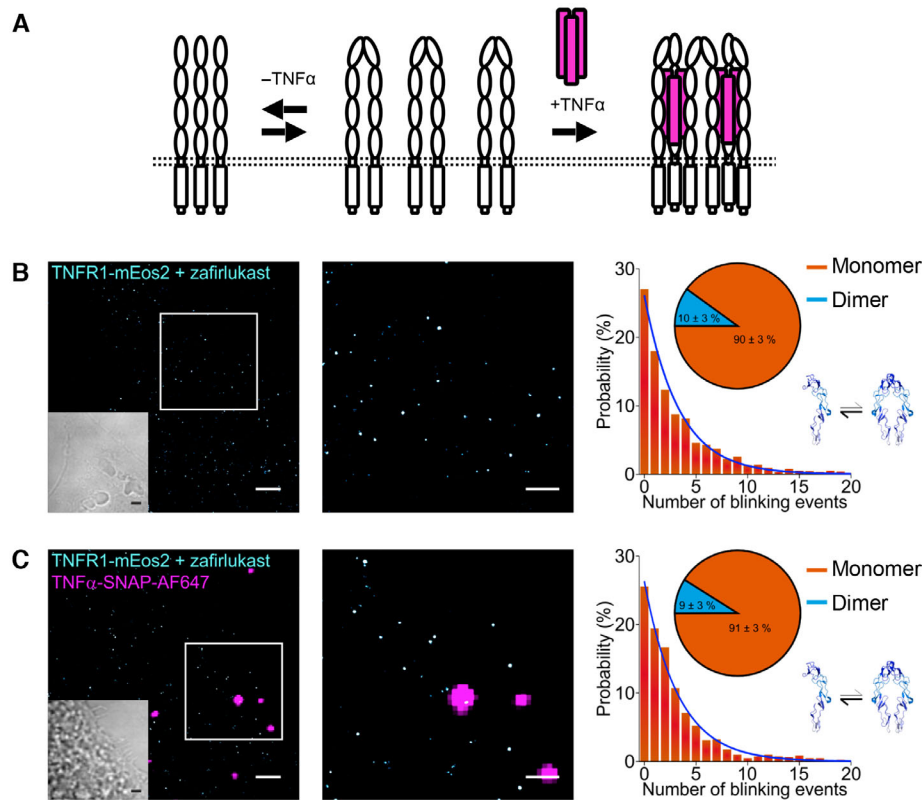


**FIGURE 1** Quantitative SMLM reveals the ligand-dependent and -independent oligomeric states of TNFR1 in the presence of zafirlukast. (A) Schematic overview of TNFR1-mEos2 distribution patterns in the mammalian cell membrane in the absence and presence of ligand, derived from Karathanasis et al.<sup>34</sup> (B and C) Shown are representative super-resolved and bright field (*gray insets*) images of TNFR1-mEos2 (*cyan*) and TNF $\alpha$ -SNAP-AF647 (*magenta*) (*left*), zoomed white-boxed regions-of-interest (*middle*) and the corresponding histograms of blinking events of mEos2-fused TNFR1 (*right*), fitted with the theoretical model functions reporting on monomer and dimer populations. TNFR1 distributions are specified in pie charts. PDB: 1NCF, 1TNF. Shown are ligand-unstimulated TNFR1-mEos2 pretreated with 100  $\mu$ M zafirlukast (B) and TNF $\alpha$ -SNAP-AF647-treated TNFR1-mEos2 pretreated with 100  $\mu$ M zafirlukast (C). Scale bars: 2  $\mu$ m for SMLM and bright field images (*left*), 1  $\mu$ m for zoomed images (*middle*). Data are based on 10 cells in each case (B and C), from 3 independent experiments

KO MEFs (Supplemental Fig. 1, lanes 4–6), suggesting that zafirlukast interferes with early TNFR1 proximal effects required for NF- $\kappa$ B signaling. Of note, the observed delay in I $\kappa$ B $\alpha$  phosphorylation in TNFR1/2 WT and TNFR1/2 KO + TNFR1-mEos2 MEFs upon zafirlukast treatment could be further reduced by cotreatment with the inhibitor of nuclear factor kappa-B kinase (IKK) inhibitor bardoxolone methyl (Fig. 2B). These observations suggest that zafirlukast inhibits NF- $\kappa$ B activation upstream of I $\kappa$ B $\alpha$  degradation.

Since TNF $\alpha$ -induced TNFR1 activation and I $\kappa$ B $\alpha$  processing culminates in NF- $\kappa$ B-mediated proinflammatory gene expression, we sought to determine the inhibitory potential of zafirlukast on TNF $\alpha$ -mediated gene expression in the reconstituted MEFs. Treating TNFR1/2 KO + TNFR1-mEos2 and TNFR1/2 WT MEFs with TNF $\alpha$  in the presence of zafirlukast prominently inhibited ligand-induced up-regulation of C-X-C motif chemokine 1 (Cxcl1), one of the mouse orthologues of human IL-8 (Fig. 2C), and I $\kappa$ B $\alpha$  (Fig. 2D) mRNA levels in TNFR1/2 KO + TNFR1-mEos2 MEFs. Zafirlukast also inhibited TNF $\alpha$ -induced Cxcl1 and I $\kappa$ B $\alpha$  mRNA in TNFR1/2 WT MEFs (Figs. 2E and 2F), but not in TNFR1/2 KO MEFs (Figs. 2G and 2H). Apart from affecting NF- $\kappa$ B-mediated gene expression, zafirlukast also potently inhibited

TNF $\alpha$ -induced Cxcl1 cytokine secretion in TNFR1/2 KO + TNFR1-mEos2 MEFs as well as in TNFR1/2 WT MEFs (Fig. 2I). As expected, and in line with the previous findings, Cxcl1 secretion in TNFR1/2 KO MEFs remains largely unaffected by TNF $\alpha$  with and without zafirlukast (Fig. 2I).

Together, these findings suggest that zafirlukast-mediated inhibition of PLAD/PLAD-dependent, ligand-independent and TNF $\alpha$ -induced TNFR1 clustering results in the inhibition of TNF $\alpha$ -induced NF- $\kappa$ B signaling. This is further underscored by the defective TNF $\alpha$ -induced NF- $\kappa$ B activation observed previously in TNFR1/2 KO + TNFR1 K32A mEos2 MEFs.<sup>34</sup> In addition, these observations also confirm the feasibility of the TNFR1/2 KO + TNFR1-mEos2 MEFs to study quantitative TNFR1 single-molecule membrane distributions as well as functional TNF $\alpha$ -induced NF- $\kappa$ B signaling responses in the same cells in single integral experimental settings at physiologic levels. In future approaches, the TNFR1-mEos2 cell lines could be further modified, for example, with fluorescently labeled I $\kappa$ B $\alpha$  or p65 to investigate dynamic NF- $\kappa$ B responses over time, or could be applied to study the relationship between TNFR1 internalization and signaling.

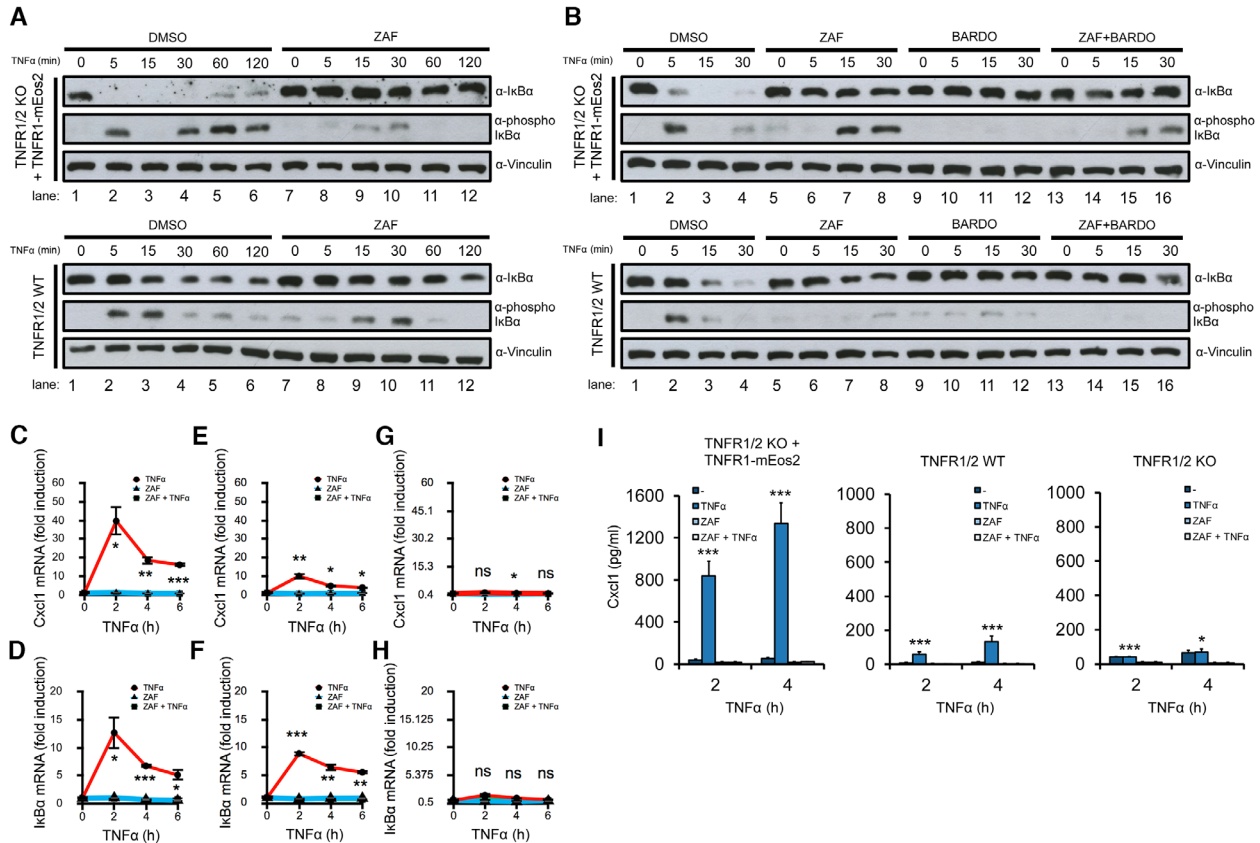


**FIGURE 2** Zafirlukast affects TNF $\alpha$ -induced NF- $\kappa$ B in TNFR1/2 WT and reconstituted TNFR1/2 KO + TNFR1 mEos2 MEFs. (A) Western blot analysis of serum-starved, DMSO-, or zafirlukast (100  $\mu$ M) treated TNFR1/2 KO + TNFR1-mEos2 MEFs (top) and TNFR1/2 WT MEFs (bottom), stimulated with TNF $\alpha$  (20 ng/ml) for the indicated time points. Membranes are probed with antibodies recognizing I $\kappa$ B $\alpha$ , phosphorylated I $\kappa$ B $\alpha$  and vinculin as loading control. Representative blots of 2 or 3 independent experiments are shown. (B) Western blot analysis of serum-starved, DMSO, zafirlukast (100  $\mu$ M) or bardoxolone methyl (1  $\mu$ M) treated TNFR1/2 KO + TNFR1-mEos2 MEFs (top) and TNFR1/2 WT MEFs (bottom), stimulated with TNF $\alpha$  (20 ng/ml) for the indicated time points. Membranes are probed with antibodies recognizing I $\kappa$ B $\alpha$ , phosphorylated I $\kappa$ B $\alpha$  and vinculin as loading control. Representative blots of 2 or 3 independent experiments are shown. (C–H) TNFR1/2 KO + TNFR1-mEos2 MEFs (C and D), TNFR1/2 WT MEFs (E and F) and TNFR1/2 KO MEFs (G and H) were pretreated with DMSO or zafirlukast (100  $\mu$ M) for 1 h at 37°C, followed by induction with TNF $\alpha$  (20 ng/ml) for the indicated time points and quantification of Cxcl1 (C, E, and G) and I $\kappa$ B $\alpha$  (D, F, and H) mRNA expression levels using qRT-PCR. Data are normalized to GAPDH and RPLP0 expression and are presented as x-fold mRNA expression compared with control. Mean and SD of 3 independent experiments performed in triplicate are shown. \* $P$  < 0.05; \*\* $P$  < 0.01; \*\*\* $P$  < 0.001, comparing TNF $\alpha$  + zafirlukast condition to conditions with TNF $\alpha$  only. (I) TNFR1/2 KO + TNFR1-mEos2, TNFR1/2 WT, and TNFR1/2 KO MEFs were pretreated with DMSO or zafirlukast (100  $\mu$ M) for 1 h at 37°C, followed by stimulation with TNF $\alpha$  (20 ng/ml) for the indicated times and quantification of absolute levels of Cxcl1 cytokine secretion using ELISA. Mean and SD of 3 independent experiments performed in triplicate are shown. \* $P$  < 0.05; \*\*\* $P$  < 0.001, TNF $\alpha$ -treated condition are compared with TNF $\alpha$  + zafirlukast-treated conditions

Next, the efficacy of zafirlukast in inhibiting TNF $\alpha$ -induced NF- $\kappa$ B responses was evaluated in the human cervical carcinoma cell line HeLa. Pretreatment with zafirlukast also induced a delay in phosphorylated I $\kappa$ B $\alpha$  and affected I $\kappa$ B $\alpha$  degradation in HeLa cells, although to a lesser extent as observed in TNFR1/2 KO + TNFR1-mEos2 MEFs, compared with solvent controls (Fig. 3A). This delay might be explained by the relative low affinity of zafirlukast for the TNFR1 PLAD and by the fact that zafirlukast is a competitive inhibitor of the PLAD.<sup>13,23</sup> Treatment of HeLa cells with TNF $\alpha$  potentially induced up-regulation of IL-8 and I $\kappa$ B $\alpha$  mRNA over time (Figs. 3B and 3C). Intriguingly, incubation with zafirlukast strongly inhibited TNF $\alpha$ -induced IL-8 and I $\kappa$ B $\alpha$  mRNA up-regulation, whereas zafirlukast treatment alone did not affect gene expression profiles, despite the delay in phosphorylated I $\kappa$ B $\alpha$  degradation (Figs. 3B and 3C). Furthermore, increasing

zafirlukast concentrations also inhibited IL-8 secretion of TNF $\alpha$ -treated HeLa cells in a dose-dependent manner (Fig. 3D), in line with inhibition of TNF $\alpha$ -induced TNFR1 clustering and alterations in I $\kappa$ B $\alpha$ . Together, these observations highlight and confirm the inhibitory effects of zafirlukast on PLAD-mediated higher-order TNFR1 clustering and TNFR1-induced NF- $\kappa$ B signaling. It would be of great interest to evaluate the efficacy of the recently identified noncompetitive TNF $\alpha$  antagonists that stabilize inactive TNFR1 conformations<sup>13</sup> in the TNFR1-mEos quantitative imaging platform.

Although the mechanistic interplay between the zafirlukast target CysLTR1 and TNFR1 signaling remains to be determined, our findings point towards an important role for PLAD-mediated ligand-independent TNFR1 dimerization and possibly PLAD-mediated clustering of TNF $\alpha$ -bound TNFR1 molecules for TNF $\alpha$ -induced TNFR1

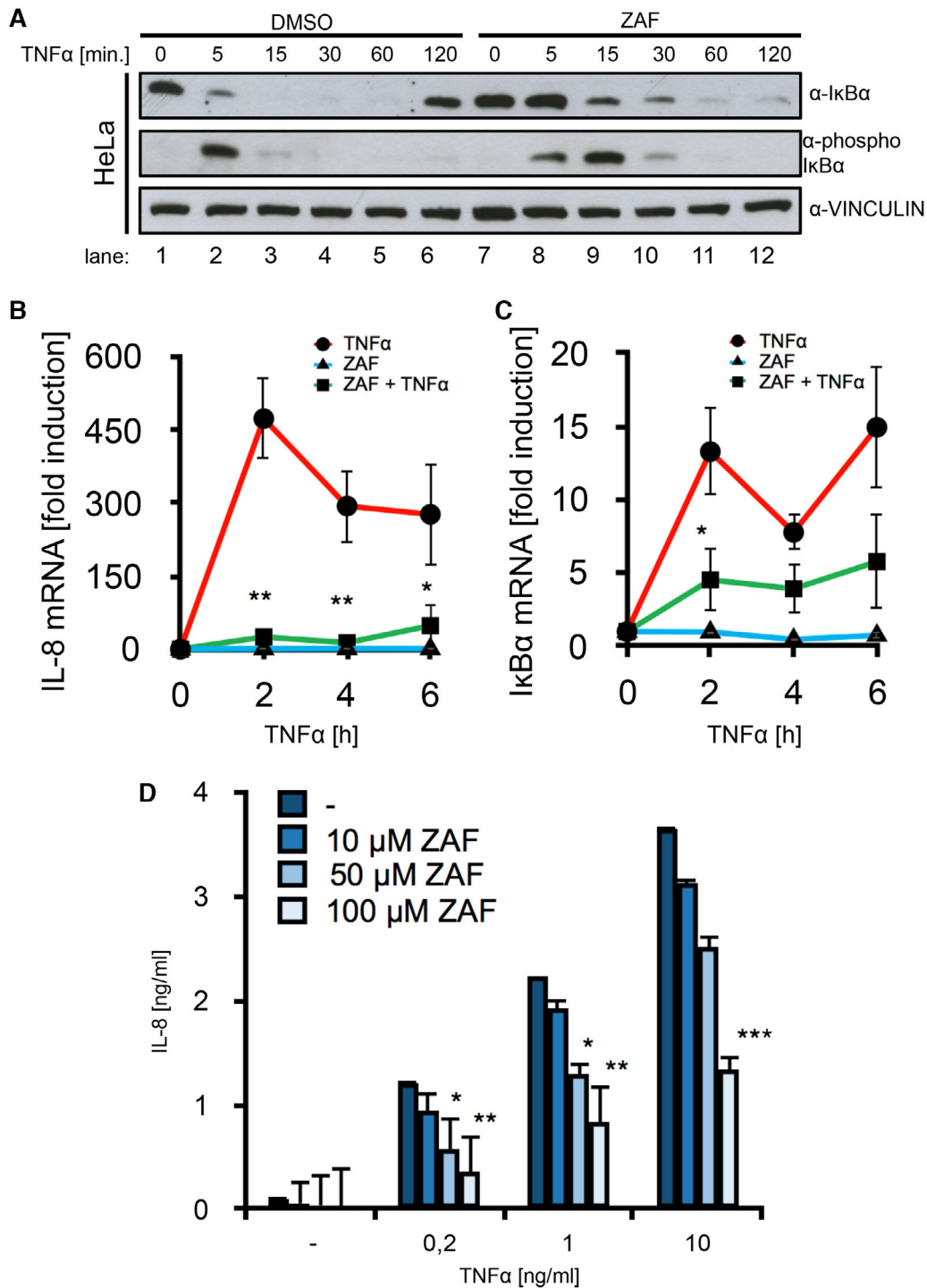


**FIGURE 3** Zafirlukast inhibits TNF $\alpha$ -induced NF- $\kappa$ B-mediated gene transcription and cytokine production in human cervical carcinoma cells. (A) Western blot analysis of serum-starved, DMSO, or zafirlukast (100  $\mu$ M) treated human cervical carcinoma (HeLa) cells, stimulated with TNF $\alpha$  (20 ng/ml) for the indicated times. Membranes are probed with antibodies recognizing I $\kappa$ B $\alpha$ , phosphorylated I $\kappa$ B $\alpha$ , and vinculin as loading control. Representative blots of 3 independent experiments are shown. (B) Human cervical carcinoma (HeLa) cells were pretreated with DMSO or zafirlukast (100  $\mu$ M) for 1 h at 37°C, followed by induction with TNF $\alpha$  (20 ng/ml) for the indicated time points and quantification of IL-8 mRNA expression levels using qRT-PCR. Data are normalized to 28S-rRNA expression and are presented as  $x$ -fold mRNA expression compared with control. Mean and SD of 3 independent experiments performed in triplicate are shown. \* $P$  < 0.05; \*\* $P$  < 0.01; comparing TNF $\alpha$  + zafirlukast condition to conditions with TNF $\alpha$  only (C) Idem as (B), but fold I $\kappa$ B $\alpha$  mRNA expression compared were quantified. Mean and SD of 3 independent experiments performed in triplicate are shown. \* $P$  < 0.05, comparing TNF $\alpha$  + zafirlukast condition to conditions with TNF $\alpha$  only (D) Human cervical carcinoma (HeLa) cells were pretreated with DMSO or zafirlukast (100  $\mu$ M) for 1 h at 37°C, followed by stimulation with TNF $\alpha$  (20 ng/ml) for the indicated times and quantification of IL-8 cytokine secretion using ELISA. Mean and SD of 3 independent experiments are shown. \* $P$  < 0.05; \*\* $P$  < 0.01; \*\*\* $P$  < 0.001, compared with conditions without zafirlukast

activation. Taken together, these observations emphasize quantitative single-molecule and single-cell TNFR1-mEos2 imaging as an attractive experimental platform to identify novel TNF $\alpha$ /TNFR1/NF- $\kappa$ B antagonists, which can be easily combined with high-throughput screening and functional analysis in one centralized assay under physiologically relevant cellular settings.

## ACKNOWLEDGMENTS

S.J.L.v.W. acknowledges funding by the DFG (WI 5171/1-1 and FU 436/20-1) and the Dr. Eberhard and Hilde Rüdiger Foundation, H.W. has been funded by the DFG (WA 1025/24-1 and TRR 221) and C.K., S.M., and M.H. acknowledge funding by the DFG (SFB 807 and SFB 1177).

## AUTHORSHIP

H.W., M.H., and S.J.L.v.W. conceptualized the study. N.W., C.K., S.S., J.M., S.M., and S.J.L.v.W. carried out all the investigations related to the study. N.W., C.K., S.S., J.M., H.W., M.H., and S.J.L.v.W. contributed with the data curation and formal analysis. N.W., C.K., S.S., J.M., S.M., S.F., H.W., M.H., and S.J.L.v.W. wrote and edited the manuscript. N.W. and C.K. contributed equally to this work.

## DISCLOSURES

The authors declare no conflicts of interest.

## ORCID

Nadine Weinelt  <https://orcid.org/0000-0002-9418-6736>  
 Christos Karathanasis  <https://orcid.org/0000-0002-1333-2341>  
 Sonja Smith  <https://orcid.org/0000-0002-7390-6917>  
 Juliane Medler  <https://orcid.org/0000-0002-9882-8433>  
 Sebastian Malkusch  <https://orcid.org/0000-0001-6766-140X>  
 Simone Fulda  <https://orcid.org/0000-0002-0459-6417>  
 Harald Wajant  <https://orcid.org/0000-0002-2005-3949>  
 Mike Heilemann  <https://orcid.org/0000-0002-9821-3578>  
 Sjoerd J. L. van Wijk  <https://orcid.org/0000-0001-6532-7651>

## REFERENCES

- Dempsey PW, Doyle SE, He JQ, Cheng G. The signaling adaptors and pathways activated by TNF superfamily. *Cytokine Growth Factor Rev.* 2003;14:193-209.
- Aggarwal BB. Signalling pathways of the TNF superfamily: a double-edged sword. *Nat Rev Immunol.* 2003;3:745-756.
- Locksley RM, Killeen N, Lenardo MJ. The TNF and TNF receptor superfamilies: integrating mammalian biology. *Cell.* 2001;104:487-501.
- Annibaldi A, Meier P. Checkpoints in TNF-induced cell death: implications in inflammation and cancer. *Trends Mol Med.* 2018;24:49-65.
- Wajant H, Scheurich P. TNFR1-induced activation of the classical NF- $\kappa$ B pathway. *FEBS J.* 2011;278:862-876.
- Vanamee ES, Faustman DL. Structural principles of tumor necrosis factor superfamily signaling. *Sci Signal.* 2018;11:pii: eaao4910.
- Banner DW, D'Arcy A, Janes W, et al. Crystal structure of the soluble human 55 kd TNF receptor-human TNF beta complex: implications for TNF receptor activation. *Cell.* 1993;73:431-445.
- Chan FK. Three is better than one: pre-ligand receptor assembly in the regulation of TNF receptor signaling. *Cytokine.* 2007;37:101-107.
- Chan FK, Chun HJ, Zheng L, Siegel RM, Bui KL, Lenardo MJ. A domain in TNF receptors that mediates ligand-independent receptor assembly and signaling. *Science.* 2000;288:2351-2354.
- Fricke F, Beaudouin J, Malkusch S, Eils R, Heilemann M. Quantitative single-molecule localization microscopy (qSMLM) of membrane proteins based on kinetic analysis of fluorophore blinking cycles. *Methods Mol Biol.* 2017;1663:115-126.
- Varfolomeev E, Blankenship JW, Wayson SM, et al. IAP antagonists induce autoubiquitination of c-IAPs, NF- $\kappa$ B activation, and TNF $\alpha$ -dependent apoptosis. *Cell.* 2007;131:669-681.
- Vince JE, Wong WW, Khan N, et al. IAP antagonists target cIAP1 to induce TNF $\alpha$ -dependent apoptosis. *Cell.* 2007;131:682-693.
- Lo CH, Schaaf TM, Grant BD, et al. Noncompetitive inhibitors of TNFR1 probe conformational activation states. *Sci Signal.* 2019;12:pii: eaav5637.
- Jarosz-Griffiths HH, Holbrook J, Lara-Reyna S, McDermott MF. TNF receptor signalling in autoimmune diseases. *Int Immunol.* 2019;31:639-648.
- Stone MB, Shelby SA, Veatch SL. Super-resolution microscopy: shedding light on the cellular plasma membrane. *Chem Rev.* 2017;117:7457-7477.
- Steele S, Libert C, Vandenbroucke RE. A new venue of TNF targeting. *Int J Mol Sci.* 2018;19:1442.
- Efimov GA, Kruglov AA, Tillib SV, Kuprash DV, Nedospasov SA. Tumor necrosis factor and the consequences of its ablation in vivo. *Mol Immunol.* 2009;47:19-27.
- Antoni C, Braun J. Side effects of anti-TNF therapy: current knowledge. *Clin Exp Rheumatol.* 2002;20:S152-157.
- Kruglov AA, Lampropoulou V, Fillatreau S, Nedospasov SA. Pathogenic and protective functions of TNF in neuroinflammation are defined by its expression in T lymphocytes and myeloid cells. *J Immunol.* 2011;187:5660-5670.
- Chung ES, Packer M, Lo KH, Fasanmade AA, Willerson JT, Anti-TNF Therapy Against Congestive Heart Failure Investigators. Randomized, double-blind, placebo-controlled, pilot trial of infliximab, a chimeric monoclonal antibody to tumor necrosis factor- $\alpha$ , in patients with moderate-to-severe heart failure: results of the anti-TNF Therapy Against Congestive Heart Failure (ATTACH) trial. *Circulation.* 2003;107:3133-3140.
- Medler J, Wajant H. Tumor necrosis factor receptor-2 (TNFR2): an overview of an emerging drug target. *Expert Opin Ther Targets.* 2019;23:295-307.
- Medler J, Nelke J, Weisenberger D, et al. TNFRSF receptor-specific antibody fusion proteins with targeting controlled Fc $\gamma$ R-independent agonistic activity. *Cell Death Dis.* 2019;10:224.
- Lo CH, Vunnam N, Lewis AK, et al. An innovative high-throughput screening approach for discovery of small molecules that inhibit TNF receptors. *SLAS Discov.* 2017;22:950-961.
- Conway SP, Etherington C, Peckham DG, Whitehead A. A pilot study of zafirlukast as an anti-inflammatory agent in the treatment of adults with cystic fibrosis. *J Cyst Fibros.* 2003;2:25-28.
- Riccioni G, Bucciarelli T, Mancini B, Di Ilio C, D'Orazio N. Antileukotriene drugs: clinical application, effectiveness and safety. *Curr Med Chem.* 2007;14:1966-1977.
- Zhou X, Cai J, Liu W, Wu X, Gao C. Cysteinyl leukotriene receptor type 1 (CysLT1R) antagonist zafirlukast protects against TNF- $\alpha$ -induced endothelial inflammation. *Biomed Pharmacother.* 2019;111:452-459.
- Sauer M, Heilemann M. Single-molecule localization microscopy in eukaryotes. *Chem Rev.* 2017;117:7478-7509.
- Fricke F, Beaudouin J, Eils R, Heilemann M. One, two or three? Probing the stoichiometry of membrane proteins by single-molecule localization microscopy. *Sci Rep.* 2015;5:14072.



29. Hummer G, Fricke F, Heilemann M. Model-independent counting of molecules in single-molecule localization microscopy. *Mol Biol Cell*. 2016;27:3637-3644.
30. Baldering TN, Bullerjahn JT, Hummer G, Heilemann M, Malkusch S. Molecule counts in complex oligomers with single-molecule localization microscopy. *J Phys D: Appl Phys*. 2019;52:474002. 474014pp.
31. Dietz MS, Heilemann M. Optical super-resolution microscopy unravels the molecular composition of functional protein complexes. *Nanoscale*. 2019;11:17981-17991.
32. Sanchez CP, Karathanasis C, Sanchez R, et al. Single-molecule imaging and quantification of the immune-variant adhesin VAR2CSA on knobs of *Plasmodium falciparum*-infected erythrocytes. *Commun Biol*. 2019;2:172.
33. Kruger CL, Zeuner MT, Cottrell GS, Widera D, Heilemann M. Quantitative single-molecule imaging of TLR4 reveals ligand-specific receptor dimerization. *Sci Signal*. 2017;10.
34. Karathanasis C, Medler J, Fricke F, et al. Single-molecule imaging reveals the oligomeric state of functional TNF $\alpha$ -induced plasma membrane TNFR1 clusters in cells. *Sci Signal*. 2020;13.
35. Wolter S, Schüttpehl M, Tscherepanow M, VAN DE Linde S, Heilemann M, Sauer M. Real-time computation of subdiffraction-resolution fluorescence images. *J Microsc*. 2010;237(1):12-22.
36. Malkusch S, Heilemann M. Extracting quantitative information from single-molecule super-resolution imaging data with LAMA - Localization Microscopy Analyzer. *Sci Rep*. 2016;6:34486.
37. Beghin A, Kechkar A, Butler C, et al. Localization-based super-resolution imaging meets high-content screening. *Nat Methods*. 2017;14:1184-1190.

#### SUPPORTING INFORMATION

Additional information may be found online in the Supporting Information section at the end of the article.

**How to cite this article:** Weinelt N, Karathanasis C, Smith S, et al. Quantitative single-molecule imaging of TNFR1 reveals zafirlukast as antagonist of TNFR1 clustering and TNF $\alpha$ -induced NF- $\kappa$ B signaling. *J Leukoc Biol*. 2021;109:363-371. <https://doi.org/10.1002/JLB.2AB0420-572RR>